

# Hybrid encoder for discrete and continuous variable QKD

Mattia Sabatini,<sup>1</sup> Tommaso Bertapelle,<sup>1</sup> Paolo Villorosi,<sup>1,2</sup> Giuseppe Vallone,<sup>1,2</sup> and Marco Avesani<sup>1,2,\*</sup>

<sup>1</sup>*Dipartimento di Ingegneria dell'Informazione, Università degli Studi di Padova, via Gradenigo 6B, 35131 Padova, Italia*

<sup>2</sup>*Padua Quantum Technologies Research Center, Università degli Studi di Padova, via Gradenigo 6A, 35131 Padova, Italy*

Quantum key distribution is emerging as a cutting-edge application of quantum technology, gradually integrating into the industrial landscape. Many protocols employing discrete or continuous variables have been developed over time. Whereas the firsts usually excel in covering longer distances, the seconds are typically superior in producing higher secret key rates at short distances. Present efforts aim to create systems that can exploit both these strengths, foreseeing the future challenge regarding the realization of a quantum network consisting of multiple and heterogeneous interconnected nodes. Within such a context, a possible solution is systems able to efficiently toggle between discrete and continuous variable working modes with hybrid quantum state encoders. Therefore, this study presents a new hybrid encoder based on an iPOGNAC modulator, ensuring compatibility with DV and CV QKD systems that can be assembled entirely with commercial-off-the-shelf components. The proposed scheme is the first supporting DV polarization protocols, thus making it an appealing candidate for space nodes of a future quantum network, given that polarization-based protocols are well suited for space links.

## I. INTRODUCTION

One of the main goals of cryptography is to enable confidential and secure communication between two parties over an un-trusted channel. To accomplish this, most existing protocols depend on computational security, meaning that they rely on mathematical problems believed to be unfeasible to solve by computers. However, this belief remains unproven, and it is conceivable that an efficient algorithm, whether classical or quantum, may exist to tackle the latter. Quantum Key Distribution (QKD) [1–3] offers a way to overcome the latter limitation by harnessing the principles of quantum mechanics. The approach enables the development of unconditionally secure protocols that can withstand adversaries possessing limitless classical or quantum computational power.

According to the degrees of freedom of the quantum phenomenon used, QKD can be categorized as Discrete Variables (DV) or Continuous Variables (CV) [4–7]. The former usually exploits single photons, such as polarization and time-bin, whereas CV uses the quadratures of the quantized electromagnetic field. The BB84 protocol pioneered DV-QKD [8]. It relies on single photon sources and non-orthogonal states for information encoding. Over time, it was refined and underwent several improvements, such as decoy states to counter photon number-splitting attacks [9] and adopting fewer states to ease practical implementation [10]. For CV-QKD, GG02 is the protocol of reference [11]. It employs Gaussian states to encode the secret key and coherent detection to measure them. However, significant practical limitations hinder its adoption, such as requiring a continuous Gaussian modulator, low reconciliation efficiency, and computationally demanding error correction procedures [12]. These challenges can be mitigated using coherent state discrete constellation modulation protocols

[13, 14]. However, this comes at the price of limiting the number of secret bits that can be encoded per symbol, affecting thus the Secret Key generation Rate (SKR) when compared to the original GG02.

Discrete and continuous protocols offer different advantages over the other. DV-QKD is known for its more mature security proofs and ability to cover longer distances, reaching a record of 421 km for a fiber-based BB84 system [15] and 1002 km using the twin-field approach [16]. Conversely, CV-QKD offers higher SKR for short lengths [17]. Yet, due to loss sensitivity, the current record distance for fiber systems is limited to 203 km [18]. Nevertheless, compared with DV-QKD, CV systems can benefit from coherent detectors and widely accessible commercial integrated telecom components. The former can work at room temperature and do not suffer from the typical Single Photon Detectors (SPDs) limitations, such as dead-time, commonly used in DV-QKD [19]; a characteristic that positively contributes to the achievable SKR. The second allows the exploitation of a widely consolidated industry, potentially enhancing the accessibility and economic viability of CV-QKD for broad adoption.

QKD initially emerged as a technology facilitating safe point-to-point communications. However, progress in the field has now reached the stage where we are beginning to witness efforts to establish QKD networks involving multiple entities [20–22]. Such a quantum network implies the presence of multiple paths, including intermediary relay nodes, linking one end user to another. Consequently, depending on the available routes and the channel's parameter connecting each node, hops may better use DV or CV protocols to maximize the overall SKR. Rather than choosing between two dedicated transmitters, a more efficient strategy is to rely on a hybrid encoder design capable of switching between DV and CV [23]. The benefits of this approach include the possibility to actively reconfigure the network characteristics in a software-defined manner, thus increasing its flexibility

\* marco.avesani@unipd.it

and improving the integration of QKD into the existing telecom infrastructure.

In this work, we present the first hybrid encoder designed to be compatible with polarization-based DV and CV QKD protocols. In fact, all the other schemes previously proposed are limited to phase-encoded and time-bin DV systems [23]. The system is realized only with fiber Commercial-Off-The-Shelf (COTS) telecom components and tested using two different setups for DV and CV, each paired with the respective receiver. The paper is structured as follows: Section II briefly outlines the working principles of the proposed hybrid encoder, Section III describe the experimental setup adopted for CV and DV operations, while in Section IV the results obtained.

## II. HYBRID QKD

### A. Applications of hybrid QKD encoders in quantum networks

Today’s telecommunication systems rely on cryptographic procedures vulnerable to adversaries holding quantum computing capabilities. This spurred research and industry to develop countermeasures like QKD, a solution devised to ensure Information Theoretic Security (ITS). However, the latter was mostly developed as a point-to-point connection requiring additional specialized infrastructure, which presents some challenges when integrating it into the current telecom grid. Moreover, such an approach encounters scaling issues for deploying QKD networks, as it is costly and increases the complexity of its management. Mitigating such issues is possible by relying on the Software Defined Network (SDN) model that is progressively embraced by telecom providers, given its ability to facilitate the integration of new services within a network infrastructure. Since the success of QKD technology, either CV or DV, will depend on the ability to integrate it within the existing infrastructures, adopting the SDN method becomes appealing due to the aforementioned benefits. Indeed, it should not impose the modification of each network device to establish a quantum link. Additionally, the routes connecting two endpoints can be easily reconfigured due to SDNs being centrally supervised. When paired with SDNs’ inherited ability for real-time network monitoring, which includes quantum metrics for the case, it enables the optimization of the SKR between parties. For instance, Hugues-Salas et al. in [24] demonstrated the ability to switch channels amid an attack, while Alia et al. in [25] showed link reorganization if the QBER exceeds a certain threshold. The aforementioned flexibility and performance can improve by letting the controller adopt DV or CV QKD protocols for a given intermediate link based on the values of the observed quantum parameters. For example, the controller can utilize CV-QKD for shorter connections as it typically offers higher

transmission rates compared to DV-QKD, while preferring the latter for longer distances due to its ability to extend much further with current technology. The method can also better adapt to the already deployed telecommunication infrastructure, which commonly employs multiple wavelengths for communication. Indeed, in such an integrated scenario, quantum and classical channels will likely share the same propagating media. A hybrid strategy can provide the SDN controller with a broader range of options to enhance node-to-node communication and organize the communication considering the particular status of the link.

Within this context, a transmitter equipped with an encoder that can generate both CV and DV quantum states and easily switch between the latter well suits the task. Moreover, such hybrid encoders may be a significantly cheaper alternative to two dedicated units while having a less complex yet compact and more adaptable design that can contribute to better system integration without compromising functionality.

### B. Hybrid CV-DV encoder

The hybrid encoder design we introduce relies on the iPOGNAC [26], a polarization modulator that showed remarkable temporal stability due to a self-compensating Sagnac loop able to counteract any drifts. The iPOGNAC’s operational principle can be understood from Figure (1). As can be seen, diagonally polarized light pulses are injected into the modulator. The input Beam Splitter (BS) acts like a circulator guiding the transmitted photons to a Polarization Beam Splitter (PBS) through a Polarization Maintaining Fiber (PMF). Then, the PBS outputs are connected to form an asymmetric Sagnac loop comprising a delay line and a phase modulator. The former enables the phase modulator to apply a different phase shift to the horizontal and vertical polarization propagating through the Sagnac loop. Indeed, the light entering the latter from the PBS vertical output travels clockwise. Upon exiting the loop, it emerges horizontally polarized with an additional “early” phase shift  $\phi_e$  induced by the phase modulator. On the other hand, the light entering through the PBS horizontal output moves counterclockwise, gains a “late” phase shift  $\phi_l$ , and exits vertically polarized. The “early” and “late” light pulses are recombined at the PBS and travel backward toward the BS. The transmitted component exits the iPOGNAC, up to a global phase, with a polarization state:

$$|\psi_{\text{out}}^{\text{POL}}\rangle = \frac{|H\rangle + e^{i(\phi_l - \phi_e)} |V\rangle}{\sqrt{2}}. \quad (1)$$

Notice that by adjusting the phases  $\phi_e$  and  $\phi_l$ , it is possible to generate any balanced superposition of horizontal and vertical polarization states.

By removing the iPOGNAC’s delay-line  $\Delta L$ , the

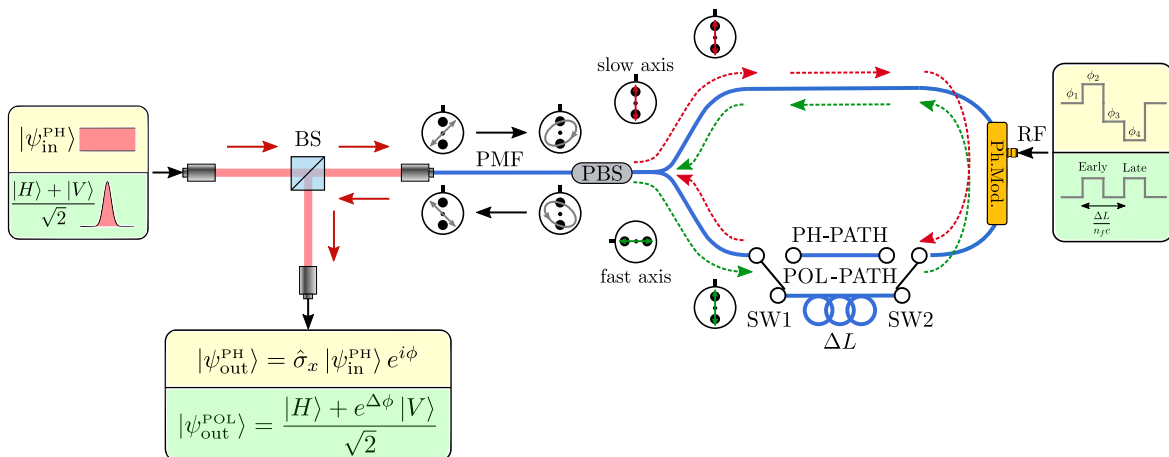


FIG. 1. A schematic representation of our proposed hybrid encoder design. The device is set in DV or CV mode according to the optical path selected: POL-PATH for the former and PH-PATH for the second. In the DV configuration, the encoder is the standard iPOGNAC in which the source is a pulsed laser aligned in such a way that the light enters the system diagonally polarized. The latter vertical and horizontal components are spatially and temporally separated by a PBS and an optical delay line  $\Delta L$  and undergo an early and late phase shift through the phase modulator. The electrical signals required to obtain such phase shifts are square pulses separated by  $n_f \Delta L/c$ , where  $n_f$  is the PMF fiber slow-axis refractive index and  $c$  is the speed of light in vacuum. In CV mode, instead, the laser source operates in CW (Continuous Wave), the  $\Delta L$  is bypassed, and by properly setting the amplitude of the electrical pulses, M-PSK modulation constellations can be obtained.

Sagnac loop is now symmetric. In this configuration, the same phase shift is applied simultaneously to both polarizations propagating through such a loop. In a left-handed reference frame whose  $z$ -axis is directed toward the photon propagation direction, the PBS and Sagnac loop map  $|H\rangle \rightarrow -|V\rangle$  and  $|V\rangle \rightarrow |H\rangle$ , which is described by the  $i\hat{\sigma}_y$  operator. If also the action of the BS is considered, then the device implements a  $\hat{\sigma}_x$  operation up to a deterministic global phase. As a result, regardless of the injected polarization state, the output is a fixed transformation of the input with an additional phase shift  $\phi$  set by the phase modulator:

$$|\psi_{\text{out}}^{\text{PH}}\rangle = \hat{\sigma}_x |\psi_{\text{in}}\rangle e^{i\phi}, \quad (2)$$

allowing thus the implementation of M-PSK (Phase Shift Keying) modulation schemes, where  $M$  is the discrete set of  $\phi$  values used. The geometry of the Sagnac loop ensures that, from the phase modulator perspective, both clockwise and counterclockwise components are always aligned with only one of its axis. This prevents the phase of the input's  $|H\rangle$  and  $|V\rangle$  components from being unevenly modulated due to the modulator's polarization-dependent characteristics. The aforementioned property is also a welcome feature since CV-QKD systems usually employ phase modulators that exhibit unwanted polarization dependency that must be controlled and stabilized with additional equipment.

Since the iPOGNAC and the CV phase encoder differ only by the optical delay line from a hardware perspective, the two can be integrated into a single system. The operational mode of this unified device mode can be set through two optical switches, SW1 and SW2, as illus-

trated in Figure (1). Indeed, the latter enables  $\Delta L$  to be bypassed. Furthermore, given that SW1 and SW2 can be electrically controllable, transitioning from DV to CV, or the reverse, can be achieved remotely with ease, in real-time, and without significant effort.

### III. EXPERIMENTAL SETUP

The capabilities of our proposed hybrid scheme were demonstrated using a DV and CV setup, each of which had its corresponding receiver.

#### A. CV setup

A schematic representation of the experimental setup used to test our hybrid encoder in CV mode is represented in Figure (2). As can be seen, a 99:1 Beam Splitter (BS-1) divides the light of a single-mode continuous-wave 1550 nm laser with a line-width of  $\sim 100$  kHz. An optical isolator (ISO) is positioned before BS-1 to prevent back-reflected light from causing laser instabilities. Then, 99% of the light from BS-1 is directed to an integrated COTS heterodyne receiver with approximately 13 dB of clearance, serving as a Local Oscillator (LO). Before entering the receiver, the light passes through a Variable Optical Attenuator (VOA-1), a Polarization Controller (PC-1), and a 99:1 Beam-Splitter (BS-2). This splitter sends 1% of the light to a monitoring Power Meter (PM-1) while the remaining 99% to the photonic chip. The power meter PM-1 and the VOA-1 are required only for calibrating the heterodyne receiver, a procedure in which we test

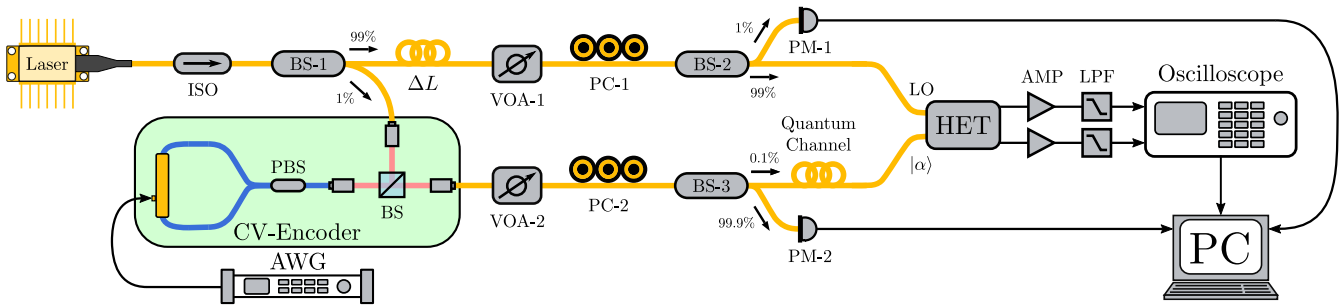


FIG. 2. Schematic representation of the CV experimental setup used. The latter consists of a 1550 nm Continuous Wave (CW) laser, the output of which is divided by a 99:1 beam-splitter (BS-1). The majority of such (99%) is directed towards a heterodyne receiver (HET) acting, thus, as a Local Oscillator (LO). The rest (1%) is sent to the CV encoder for CV quantum state phase modulation and then routed, through a fiber quantum channel, to the heterodyne’s signal input port. Subsequently, the heterodyne measurements are digitized by an oscilloscope and delivered to a PC for data processing. Notice that additional optical components are present between the 99% BS-1 arm and the HET, as well as between the CV encoder and the HET. The former are required to characterize the heterodyne receiver (such as photodiode linearity and clearance), while the latter attenuate the modulated coherent state generated by the encoder to the quantum level. Finally, the image provides a color-coded representation of the fibers used: blue for single-mode polarization-maintaining and yellow for single-mode non-polarization-maintaining.

the linearity of its photodiodes and estimate the parameters to convert the measured heterodyne signals from volt units into shot-noise units. The polarization controller, instead, is necessary to maximize the amount of optical power coupled into the chip due to the LO inlet being polarization-sensitive. Conversely, the BS-1 1% branch sends the light to the hybrid encoder configured to work in CV. The light from this encoder then travels through VOA-2, the polarization controller PC-2, and the 99.9:0.1 BS-3. Given the dual-polarization feature of the heterodyne receiver, PC-2 aligns the light polarization state to ensure that only one of the two polarization-dependent heterodyne is used. Moreover, with this cascade we can attenuate the incoming light to the required quantum level and monitor such with the PM-2 power meter at the 99.9% branch of BS-3. The BS-3 0.1% branch is subsequently connected to the heterodyne’s signal input port through a quantum channel. Notice that the signal and LO paths share the same 1550 nm laser and maintain identical lengths, with additional  $\Delta L$  fiber at the LO branch, to minimize phase noise and instabilities at the receiver. Since our objective is to evaluate our CV encoding scheme, this approach eases the experimental implementation compared to the more secure Local-Local oscillator technique [27, 28]. After detection, the electrical signals from the integrated chip are amplified using two RF amplifiers and subsequently filtered by two RF low-pass filters. Each RF component has a bandwidth of 500 MHz. Then, these signals are digitized by a 4 GHz oscilloscope with a resolution of 8-bit and a sampling rate of 25 GS/s. Finally, the digitized data is streamed to a computer for further offline analysis. The latter procedure accounts for constellation reconstruction and estimation of the main encoder parameters for CV-QKD, i.e. electronic noise, excess noise, and transmittance. To test the performance of our CV encoder, we used the

$\phi$ -phase shifts  $\pi/2$ ,  $3\pi/2$ ,  $-3\pi/2$  and  $-\pi/2$ . The electrical control signals were generated by a 16-bit Arbitrary Waveform Generator (AWG) operating at a symbol rate of 50 MBaud. To simplify post-processing, we synced the oscilloscope’s data acquisition with the AWG via a reference clock.

## B. DV setup

The experimental DV setup used is similar to the one described in [29] for the transmitter, and to the one detailed in [30] for the receiver. The source is a 1550 nm gain-switched laser emitting phase randomized pulses with a temporal width of 270 ps, measured at full-width-half-maximum, with a repetition rate of 50 MHz. The pulse amplitude is then modulated with a Sagnac interferometer [31], which includes a 70:30 BS, a phase modulator, and an optical delay line of one meter. This Sagnac modulator is employed to generate the decoy states. Before entering the iPOGNAC, the polarization of the light pulse is rotated to guarantee that it enters diagonally polarized. We obtain such by rotating the iPOGNAC’s input fiber collimator. Subsequently, the pulse polarization is adjusted using an iPOGNAC to produce the state  $|D\rangle$  (diagonal),  $|R\rangle = (|H\rangle - i|V\rangle)/\sqrt{2}$  (circular right-handed), and  $|L\rangle = (|H\rangle + i|V\rangle)/\sqrt{2}$  (circular left-handed) by setting  $\phi_l - \phi_e$  respectively equal to 0,  $-\pi/2$ , and  $+\pi/2$ . Before being sent to the receiver through a fiber quantum channel with  $\sim 6.6$  dB of losses, these states are attenuated to the single-photon level by a calibrated VOA and filtered with a narrow-band optical filter centered at 1550.12 nm to reduce noise. The receiver then detects the incoming states by randomly alternating between the basis sets  $\{|D\rangle, |A\rangle\}$  (check basis) and  $\{|R\rangle, |L\rangle\}$  (key basis), each with an equal probabil-

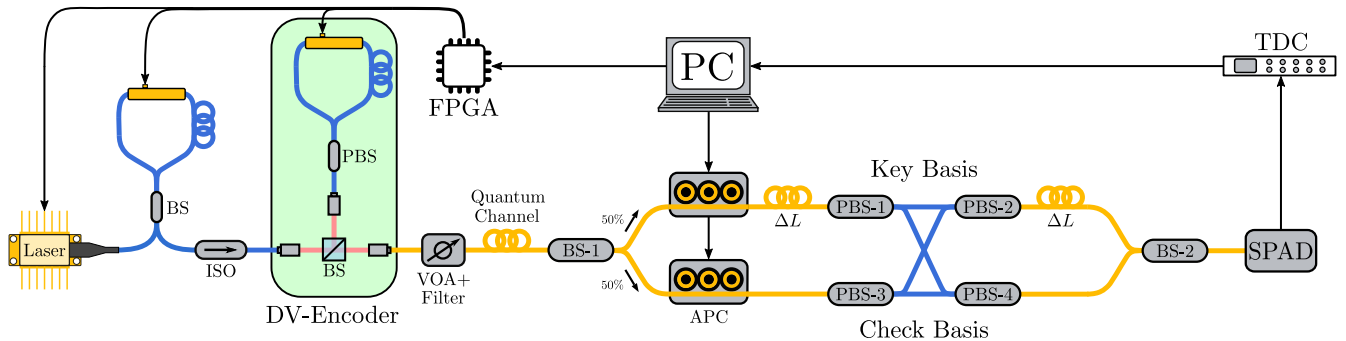


FIG. 3. The system employs a 1550 nm pulsed laser, modulated by a Sagnac interferometer and iPOGNAC for decoy and quantum states  $|D\rangle$ ,  $|R\rangle$ ,  $|L\rangle$  generation respectively. To guarantee that the iPOGNAC outputs  $|D\rangle$ ,  $|R\rangle$ ,  $|L\rangle$ , the input light must be  $|D\rangle$ , a condition achieved by carefully aligning such polarization modulator with the Sagnac, and the phase modulator must be operated with the appropriate electrical signals. The light is then attenuated to the single photon level by a Variable Optical Attenuator (VOA), filtered by a narrow-band optical filter centered at 1550.12 nm to reject noise, and directed, through a fiber quantum channel, to a time-multiplexed receiver with a Single Photon Avalanche Detector (SPAD) and two Automatic Polarization Controller (APDs) for QKD measurement. Finally, a time-tagger (TDC) records the SPAD signals for PC analysis. Notice that the signals controlling the Laser, Sagnac, and iPOGNAC are managed by an FPGA to ensure the correct timings. Moreover, the image provides a color-coded representation of the fibers used: blue for single-mode polarization-maintaining and yellow for single-mode non-polarization-maintaining fibers.

ity of selection. Such selection is passively realized using a 50:50 BS, and each projective measurement is implemented with an automatic polarization controller and a PBS. Moreover, a time and polarization multiplexing scheme performs the measurements using only one In-GaAs/InP Single-Photon Avalanche Detector (SPAD). Finally, the photon's time-of-arrival is recorded by a Time-to-Digital-Converter (TDC), and the time synchronization is performed through the Qubit4Sync algorithm, using the qubits from the quantum communication [32].

#### IV. RESULTS

In the experiment with the CV phase encoder, we repeatedly transmitted four coherent states that formed a QPSK constellation. Figure (4) depicts an example of the received constellation when Alice's modulation variance is approximately 12.4 SNU. Such a value is not suited for CV-QKD purposes. However, it allows us to resolve the constellation enough to showcase the encoder's modulation capabilities. For CV-QKD applications, the employed variance  $V_A$  is detailed in Table (I).

Table (I) reports the parameters estimated for our phase encoder. Assuming a trusted detector scenario, the heterodyne receiver was calibrated estimating its electric noise  $V_{el}$  and losses  $\eta$  (the product of the efficiency of its photodetectors and transmittance) which resulted approximately 0.081 SNU and 0.27 respectively. The modulation variance  $V_A$  of the symbols transmitted by Alice was measured by the power meter PM-2 giving the value  $\sim 0.45$  SNU (we recall that such quantity is related to the mean photon number  $\mu$  of the generated states as  $V_A = 2\mu$ ). The excess noise parameter  $\xi_A$  and channel

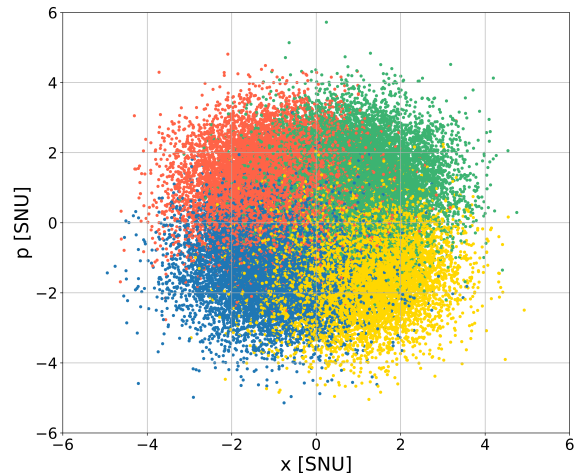


FIG. 4. The picture showcases an example of QPSK constellation obtained with our CV-Encoder operating at a symbol rate of 50 MBaud and with Alice's variance  $V_A$  set to  $\sim 12.4$  SNU.

transmittance  $T$  were obtained by the following relations:

$$\langle X_A X_B \rangle = \sqrt{\frac{\eta T}{2}} V_A \quad (3)$$

$$V_B = 1 + V_{el} + \frac{\eta T}{2} V_A + \frac{\eta T}{2} \xi_A \quad (4)$$

with  $\langle X_A X_B \rangle$  the covariance matrix elements and  $V_B$  Bob's variance estimated by analyzing a dataset of  $1.5 \cdot 10^6$  symbols acquired with the oscilloscope. The ideal asymptotic SKR obtained with our device is approxi-

Parameter	Symbol	Value	Units
Electronic noise variance	$V_{el}$	0.081	SNU
Receiver losses	$\eta$	0.30	
Alice's variance	$V_A$	0.45	SNU
Channel transmittance	$T$	0.72	
Excess noise	$\xi_A$	0.012	SNU
Asymptotic Secret Key Rate	SKR	0.026	bits/symbol

TABLE I. Values of the parameter estimation using the CV-Encoder with 50 MBaud QPSK modulation and setting the information reconciliation efficiency to 95%. The results are obtained by analyzing 30 samples, each with 50 000 symbols.

mately 0.026 bits/symbol, which leads, given a symbol-rate of 50 MBaud, to a bit-rate of  $\sim 1.3$  Mbps. To compute the latter, we use the well-known Devetak-Winter bound [33]  $SKR = \beta I_{AB} - \chi_E$ , where  $\beta$  set at a value of 95% (typically employed in the literature [14, 34]) is the error correction efficiency,  $I_{AB}$  is the mutual information between Alice and Bob, and  $\chi_E$  the Holevo bound on the information between Bob and Eve in the reverse reconciliation scenario. To compute the Holevo bound  $\chi_E$ , we relied on the Linear Channel (LC) model security analysis detailed in Ref. [13, 35]. Such an approach restricts the possible attacks performed by the eavesdropper. Nonetheless, these limitations are overcome with a newly developed theory based on Semi-Definite Programming (SDP) [14, 36]. Despite the advantages, currently, the latter does not consider hardware non-idealities like the electronic noise  $V_{el}$  and the detector efficiency  $\eta$ . In both cases, the tolerable excess noise for QPSK is very low, limiting the SKR and reachable distances. Improving the latter requires larger constellation schemes [14, 37].

For the DV encoder, we estimated the QBER and SKR when implementing the efficient three-states one-decoy protocol. The results are shown in Figure (5). As can be seen, the finite-size SKR shows very high stability during 24 hours of data acquisition, with an average of 4.7 kbps. This is further demonstrated by the intrinsic QBER plot, which remains very low with an average of 0.6% for both bases. The results further confirm the excellent performance of the iPOGNC as a polarization encoder in terms of QBER and long term stability.

## V. CONCLUSIONS

Hybrid QKD systems are powerful tools for managing a complex quantum network. When paired with the functionalities provided by an SDN, these systems can enable a more flexible and optimized allocation of its resources. Such versatility is largely due to their ability

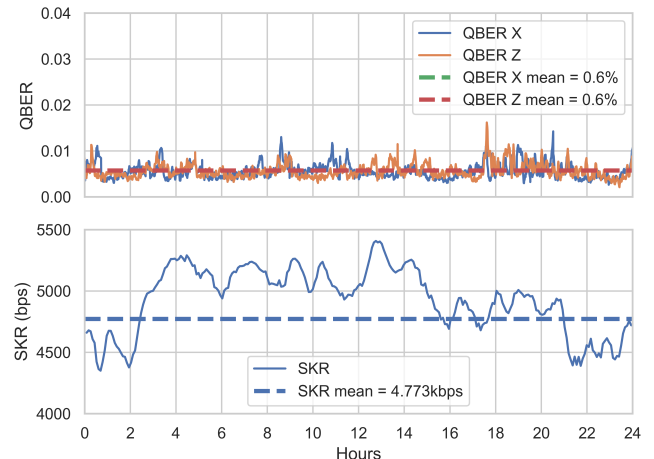


FIG. 5. The picture illustrates the performance achieved during 24 hours of continuous operation with our hybrid encoder in DV mode. The upper panel displays the QBER for both the key (Z) and check (X) basis, averaging 0.6% in each case. The lower panel shows the associated finite-size SKR, which averages 4.7 kbps.

to toggle between DV and CV protocols, which is fundamental for implementing these networks. In this work, we present a hybrid encoder to support both CV and polarization-based DV QKD protocols, which, to the best of our knowledge, is the first of its kind. Our approach leverages an iPOGNC for DV, where the polarization encoder's Sagnac loop is asymmetric due to an optical delay line, and for CV applications, in which the loop is symmetric as the previously mentioned delay is bypassed. We remark that since we are exploiting a Sagnac loop, all perturbations are canceled. This feature improves the QBER for DV-QKD and renders the encoder polarization-insensitive for CV systems. Specifically, in the DV setup, we obtained a low QBER of  $\sim 0.6\%$  over 24 hours and a finite-size SKR of  $\sim 4.7$  kbps. For the CV scenario, the excess noise is measured around 1%, with an asymptotic SKR of almost 0.026 bits/symbol, which, with the employed symbol-rate of 50 MBaud used, translates to a bit-rate of  $\sim 1.3$  Mbps.

Considering the compatibility of our device with established space DV protocols, which are usually polarization-based, and the high interest on the development of CV-QKD systems for space, our device becomes an attractive solution. On top of this, such solution that allows to combine both CV and DV encoders enabling also to reduce size, power, and cost over dedicated encoder schemes.

In conclusion, this work introduces a hybrid encoder compatible with CV and polarization-based DV QKD protocols built entirely from COTS components. Furthermore, it features high stability alongside polarization insensitivity, and by integrating supplementary external components, it can also support additional phase-based DV protocols. We believe that our design repre-

sents an advancement in the realization of flexible and re-configurable nodes for the quantum networks of the future in which simplicity and compactness also matter.

### ACKNOWLEDGMENTS

The authors would like to thank Dr. Matteo Schiavon and Dr. Yoann Piétri for the useful discussions.

We also thank the CloudVeneto facility for computational resources. Part of this work was supported by the European Union’s Horizon Europe research and innovation programme under the project QUANGO (grant agreement No 101004341) and the project “Quantum Secure Networks Partnership” (QSNP, grant agreement No 101114043).

- 
- [1] V. Scarani, H. Bechmann-Pasquinucci, N. J. Cerf, M. Dušek, N. Lütkenhaus, and M. Peev, The security of practical quantum key distribution, *Reviews of Modern Physics* **81**, 1301 (2009), publisher: American Physical Society.
- [2] N. Gisin, G. Ribordy, W. Tittel, and H. Zbinden, Quantum cryptography, *Reviews of Modern Physics* **74**, 145 (2002), publisher: American Physical Society.
- [3] F. Xu, X. Ma, Q. Zhang, H.-K. Lo, and J.-W. Pan, Secure quantum key distribution with realistic devices, *Reviews of Modern Physics* **92**, 025002 (2020), publisher: American Physical Society.
- [4] C. Weedbrook, S. Pirandola, R. García-Patrón, N. J. Cerf, T. C. Ralph, J. H. Shapiro, and S. Lloyd, Gaussian quantum information, *Reviews of Modern Physics* **84**, 621 (2012), publisher: American Physical Society.
- [5] F. Laudenbach, C. Pacher, C.-H. F. Fung, A. Poppe, M. Peev, B. Schrenk, M. Hentschel, P. Walther, and H. Hübel, Continuous-Variable Quantum Key Distribution with Gaussian Modulation—The Theory of Practical Implementations (Adv. Quantum Technol. 1/2018), *Advanced Quantum Technologies* **1**, 1870011 (2018).
- [6] S. Pirandola, U. L. Andersen, L. Banchi, M. Berta, D. Bunandar, R. Colbeck, D. Englund, T. Gehring, C. Lupo, C. Ottaviani, J. L. Pereira, M. Razavi, J. S. Shaari, M. Tomamichel, V. C. Usenko, G. Vallone, P. Villoresi, and P. Wallden, Advances in quantum cryptography, *Advances in Optics and Photonics* **12**, 1012 (2020), publisher: Optica Publishing Group.
- [7] Y. Zhang, Y. Bian, Z. Li, S. Yu, and H. Guo, Continuous-variable quantum key distribution system: Past, present, and future, *Applied Physics Reviews* **11**, 011318 (2024).
- [8] C. H. Bennett and G. Brassard, Quantum cryptography: Public key distribution and coin tossing, *Theoretical Computer Science* **560**, 7 (2014), theoretical Aspects of Quantum Cryptography – celebrating 30 years of BB84.
- [9] G. Brassard, N. Lütkenhaus, T. Mor, and B. C. Sanders, Limitations on Practical Quantum Cryptography, *Physical Review Letters* **85**, 1330 (2000), publisher: American Physical Society.
- [10] F. Grünenfelder, A. Boaron, D. Rusca, A. Martin, and H. Zbinden, Simple and high-speed polarization-based QKD, *Applied Physics Letters* **112**, 051108 (2018).
- [11] F. Grosshans and P. Grangier, Continuous Variable Quantum Cryptography Using Coherent States, *Physical Review Letters* **88**, 057902 (2002), publisher: American Physical Society.
- [12] M. Almeida, D. Pereira, N. J. Muga, M. Facão, A. N. Pinto, and N. A. Silva, Secret key rate of multi-ring M-APSK continuous variable quantum key distribution, *Optics Express* **29**, 38669 (2021), publisher: Optica Publishing Group.
- [13] A. Leverrier and P. Grangier, Unconditional Security Proof of Long-Distance Continuous-Variable Quantum Key Distribution with Discrete Modulation, *Physical Review Letters* **102**, 180504 (2009), publisher: American Physical Society.
- [14] A. Denys, P. Brown, and A. Leverrier, Explicit asymptotic secret key rate of continuous-variable quantum key distribution with an arbitrary modulation, *Quantum* **5**, 540 (2021), publisher: Verein zur Förderung des Open Access Publizierens in den Quantenwissenschaften.
- [15] A. Boaron, G. Boso, D. Rusca, C. Vulliez, C. Autebert, M. Caloz, M. Perrenoud, G. Gras, F. Bussièeres, M.-J. Li, D. Nolan, A. Martin, and H. Zbinden, Secure Quantum Key Distribution over 421 km of Optical Fiber, *Physical Review Letters* **121**, 190502 (2018), publisher: American Physical Society.
- [16] Y. Liu, W.-J. Zhang, C. Jiang, J.-P. Chen, C. Zhang, W.-X. Pan, D. Ma, H. Dong, J.-M. Xiong, C.-J. Zhang, H. Li, R.-C. Wang, J. Wu, T.-Y. Chen, L. You, X.-B. Wang, Q. Zhang, and J.-W. Pan, Experimental Twin-Field Quantum Key Distribution over 1000 km Fiber Distance, *Physical Review Letters* **130**, 210801 (2023), publisher: American Physical Society.
- [17] R. Asif and W. J. Buchanan, Seamless cryptographic key generation via off-the-shelf telecommunication components for end-to-end data encryption, in *2017 IEEE International Conference on Internet of Things (iThings) and IEEE Green Computing and Communications (GreenCom) and IEEE Cyber, Physical and Social Computing (CPSCom) and IEEE Smart Data (SmartData)* (2017) pp. 910–916.
- [18] Y. Zhang, Z. Chen, S. Pirandola, X. Wang, C. Zhou, B. Chu, Y. Zhao, B. Xu, S. Yu, and H. Guo, Long-Distance Continuous-Variable Quantum Key Distribution over 202.81 km of Fiber, *Physical Review Letters* **125**, 010502 (2020), publisher: American Physical Society.
- [19] X.-J. Huang, F.-Y. Lu, S. Wang, Z.-Q. Yin, Z.-H. Wang, W. Chen, D.-Y. He, G.-J. Fan-Yuan, G.-C. Guo, and Z.-F. Han, Dependency model for high-performance quantum-key-distribution systems, *Physical Review A* **106**, 062607 (2022), publisher: American Physical Society.
- [20] M. Peev, C. Pacher, R. Alléaume, C. Barreiro, J. Bouda, W. Boxleitner, T. Debuisschert, E. Diamanti, M. Dianati, J. F. Dynes, S. Fasel, S. Fossier, M. Fürst, J.-D. Gautier, O. Gay, N. Gisin, P. Grangier, A. Happe, Y. Hasani,

- M. Hentschel, H. Hübel, G. Humer, T. Länger, M. Legré, R. Lieger, J. Lodewyck, T. Lorünser, N. Lütkenhaus, A. Marhold, T. Matyus, O. Maurhart, L. Monat, S. Nauerth, J.-B. Page, A. Poppe, E. Querasser, G. Ribordy, S. Robyr, L. Salvail, A. W. Sharpe, A. J. Shields, D. Stucki, M. Suda, C. Tamas, T. Themel, R. T. Thew, Y. Thoma, A. Treiber, P. Trinkler, R. Tualle-Brouiri, F. Vannel, N. Walenta, H. Weier, H. Weinfurter, I. Wimberger, Z. L. Yuan, H. Zbinden, and A. Zeilinger, The SECOQC quantum key distribution network in Vienna, *New Journal of Physics* **11**, 075001 (2009).
- [21] M. Sasaki, M. Fujiwara, H. Ishizuka, W. Klaus, K. Wakui, M. Takeoka, S. Miki, T. Yamashita, Z. Wang, A. Tanaka, K. Yoshino, Y. Nambu, S. Takahashi, A. Tajima, A. Tomita, T. Domeki, T. Hasegawa, Y. Sakai, H. Kobayashi, T. Asai, K. Shimizu, T. Tokura, T. Tsurumaru, M. Matsui, T. Honjo, K. Tamaki, H. Takesue, Y. Tokura, J. F. Dynes, A. R. Dixon, A. W. Sharpe, Z. L. Yuan, A. J. Shields, S. Uchikoga, M. Legré, S. Robyr, P. Trinkler, L. Monat, J.-B. Page, G. Ribordy, A. Poppe, A. Allacher, O. Maurhart, T. Länger, M. Peev, and A. Zeilinger, Field test of quantum key distribution in the Tokyo QKD Network, *Optics Express* **19**, 10387 (2011), publisher: Optica Publishing Group.
- [22] A. Aguado, V. Lopez, D. Lopez, M. Peev, A. Poppe, A. Pastor, J. Folgueira, and V. Martin, The Engineering of Software-Defined Quantum Key Distribution Networks, *IEEE Communications Magazine* **57**, 20 (2019), conference Name: IEEE Communications Magazine.
- [23] I. H. L. Grande, S. Etcheverry, J. Aldama, S. Ghasemi, D. Nolan, and V. Pruneri, Adaptable transmitter for discrete and continuous variable quantum key distribution, *Optics Express* **29**, 14815 (2021), publisher: Optica Publishing Group.
- [24] E. Hugues-Salas, F. Ntavou, D. Gkounis, G. T. Kanellos, R. Nejabati, and D. Simeonidou, Monitoring and physical-layer attack mitigation in SDN-controlled quantum key distribution networks, *Journal of Optical Communications and Networking* **11**, A209 (2019), conference Name: Journal of Optical Communications and Networking.
- [25] O. Alia, R. S. Tessinari, E. Hugues-Salas, G. T. Kanellos, R. Nejabati, and D. Simeonidou, Dynamic DV-QKD Networking in Trusted-Node-Free Software-Defined Optical Networks, *Journal of Lightwave Technology* **40**, 5816 (2022), publisher: IEEE.
- [26] M. Avesani, C. Agnesi, A. Stanco, G. Vallone, and P. Villoresi, Stable, low-error, and calibration-free polarization encoder for free-space quantum communication, *Optics Letters* **45**, 4706 (2020), publisher: Optica Publishing Group.
- [27] D. B. Soh, C. Brif, P. J. Coles, N. Lütkenhaus, R. M. Camacho, J. Urayama, and M. Sarovar, Self-Referenced Continuous-Variable Quantum Key Distribution Protocol, *Physical Review X* **5**, 041010 (2015), publisher: American Physical Society.
- [28] B. Qi, P. Lougovski, R. Pooser, W. Grice, and M. Bobrek, Generating the Local Oscillator “Locally” in Continuous-Variable Quantum Key Distribution Based on Coherent Detection, *Physical Review X* **5**, 041009 (2015), publisher: American Physical Society.
- [29] M. Avesani, L. Calderaro, G. Foletto, C. Agnesi, F. Picciariello, F. B. L. Santagiustina, A. Scriminich, A. Stanco, F. Vedovato, M. Zahidy, G. Vallone, and P. Villoresi, Resource-effective quantum key distribution: a field trial in Padua city center, *Optics Letters* **46**, 2848 (2021), publisher: Optica Publishing Group.
- [30] M. Avesani, G. Foletto, M. Padovan, L. Calderaro, C. Agnesi, E. Bazzani, F. Berra, T. Bertapelle, F. Picciariello, F. B. L. Santagiustina, D. Scalcon, A. Scriminich, A. Stanco, F. Vedovato, G. Vallone, and P. Villoresi, Deployment-Ready Quantum Key Distribution Over a Classical Network Infrastructure in Padua, *Journal of Lightwave Technology* **40**, 1658 (2022), conference Name: Journal of Lightwave Technology.
- [31] G. L. Roberts, M. Pittaluga, M. Minder, M. Lucamarini, J. F. Dynes, Z. L. Yuan, and A. J. Shields, Patterning-effect-free intensity modulator for secure decoy-state quantum key distribution, *Optics Letters* **43**, 5110 (2018), arXiv:1807.07414 [quant-ph].
- [32] L. Calderaro, A. Stanco, C. Agnesi, M. Avesani, D. Dequal, P. Villoresi, and G. Vallone, Fast and Simple Qubit-Based Synchronization for Quantum Key Distribution, *Physical Review Applied* **13**, 054041 (2020), publisher: American Physical Society.
- [33] I. Devetak and A. Winter, Distillation of secret key and entanglement from quantum states, *Proceedings of the Royal Society A: Mathematical, Physical and Engineering Sciences* **461**, 207 (2005), publisher: Royal Society.
- [34] H. Wang, Y. Li, Y. Pi, Y. Pan, Y. Shao, L. Ma, Y. Zhang, J. Yang, T. Zhang, W. Huang, and B. Xu, Sub-Gbps key rate four-state continuous-variable quantum key distribution within metropolitan area, *Communications Physics* **5**, 1 (2022), number: 1 Publisher: Nature Publishing Group.
- [35] H. Zhang, J. Fang, and G. He, Improving the performance of the four-state continuous-variable quantum key distribution by using optical amplifiers, *Physical Review A* **86**, 022338 (2012), publisher: American Physical Society.
- [36] S. Ghorai, P. Grangier, E. Diamanti, and A. Leverrier, Asymptotic Security of Continuous-Variable Quantum Key Distribution with a Discrete Modulation, *Physical Review X* **9**, 021059 (2019), publisher: American Physical Society.
- [37] W. Zhao, R. Shi, Y. Feng, and D. Huang, Unidimensional continuous-variable quantum key distribution with discrete modulation, *Physics Letters A* **384**, 126061 (2020).